

# Nanoscale

Accepted Manuscript



This is an *Accepted Manuscript*, which has been through the Royal Society of Chemistry peer review process and has been accepted for publication.

*Accepted Manuscripts* are published online shortly after acceptance, before technical editing, formatting and proof reading. Using this free service, authors can make their results available to the community, in citable form, before we publish the edited article. We will replace this *Accepted Manuscript* with the edited and formatted *Advance Article* as soon as it is available.

You can find more information about *Accepted Manuscripts* in the [Information for Authors](#).

Please note that technical editing may introduce minor changes to the text and/or graphics, which may alter content. The journal's standard [Terms & Conditions](#) and the [Ethical guidelines](#) still apply. In no event shall the Royal Society of Chemistry be held responsible for any errors or omissions in this *Accepted Manuscript* or any consequences arising from the use of any information it contains.



## Nanoscale

## ARTICLE

## Tailoring the transmission lineshape spectrum of zigzag graphene nanoribbon based heterojunctions via controlling its width and edge protrusions

Received 00th January 20xx,  
Accepted 00th January 20xx

DOI: 10.1039/x0xx00000x

[www.rsc.org/](http://www.rsc.org/)

K. P. Dou,<sup>a</sup> X. X. Fu,<sup>a</sup> Abir De Sarkar<sup>b</sup> and R. Q. Zhang<sup>\*a</sup>

We report a first-principles analysis of electron transport through narrow zigzag graphene nanoribbon (up to 2.2 nm) based wedge-shaped heterojunctions. We show that width difference between the electrode and the scattering region and the edge protrusion of heterojunctions can be tuned to endow the system's transmission spectrum with distinctive features. In particular, transport through junctions with one sided protrusion in the scattering region is always dominated by a Breit-Wigner-type resonance right at the Fermi level, regardless of the large or small width difference. On the other hand, junction with protrusions on both sides of the scattering region shows insulating behaviour near the Fermi level for large width difference but weak transmission channels are formed at the core of the scattering region for small width difference. When protrusion is absent in the junction, transmission functions display rather complex structures: double-peak away from Fermi level and strongly asymmetric profile in the vicinity of Fermi level are observed for large and small width difference, respectively. These results may shed light in designing real connecting components in nano circuits.

### Introduction

Conventional integrated circuits are designed in two steps: fabricating all necessary discrete electrical components and wiring from silicon, and then integrating all these elements in the same silicon wafer. Recently, owing to an intense surge in interest in carbon materials such as graphene, its great potential for application in future nanoelectronics<sup>1,2</sup> is also being explored. Graphene is a single atomic layer of graphite<sup>3</sup> and can potentially offer a robust building block analogous to the silicon transistor. Besides, its seamless coupling to incorporate these functional carbon based nanounits through graphene nanoribbon (GNR) interconnects will in turn allow for ballistic transport.

A pristine graphene sheet does not have a finite energy gap but band gaps<sup>4</sup> can be controllably opened through a simple variation in graphene, viz. designing nanoribbons with desired widths in order to fabricate field-effect transistors (FETs) with desirable on-off ratios. GNRs have attracted intensive research interests because of quasi one dimensional and fascinating electronic properties. Generally, two routes are adopted to fine tune their electronic structures and then apply them to the basic units in nanoelectronics: chemical modifications<sup>5-10</sup> and edge modifications.<sup>10-16</sup>

Wang *et al.*<sup>5</sup> found that the chemical modification of armchair GNRs (AGNRs) results in a considerable deformation of the bond lengths and angles near the edge and lead to observable metal-to-insulator transitions. Hod *et al.*<sup>6</sup> reported higher stability of edge-oxidized zigzag GNRs (ZGNRs) than hydrogen-terminated ones except for the case of the etheric groups. Geunsik *et al.*<sup>7</sup> also found ZGNRs with edge oxidation to be energetically more favorable than those with hydrogen passivation, while edge oxidized GNRs show metallic band structures caused by the larger electronegativity of oxygen relative to carbon. Zheng *et al.*<sup>8</sup> indicated that saturating zigzag edges of the graphene nanodots with different atoms or molecular groups could provide an opportunity to tailor 0D graphene nanostructures for applications as molecular sensors and transistor devices. Blanca *et al.*<sup>9</sup> reported nitrogen doped AGNRs to exhibit strong electron-hole conduction asymmetry which could be used to improve the performances of graphene based FETs.

Interestingly, modifications in edge geometry of GNRs can also bring about such strong electron-hole conduction asymmetry. For example, single topological defects such as pentagons (heptagons) develop a marked acceptor (donor) character in the transport properties of

<sup>a</sup>Department of Physics and Materials Science, City University of Hong Kong, Hong Kong SAR E-mail: [opraqz@cityu.edu.hk](mailto:opraqz@cityu.edu.hk)

<sup>b</sup>Computational Nanoscience Group, Institute of Nano Science and Technology (An Autonomous Institute supported by the Department of Science and Technology, Government of India), Habitat Centre, Phase X, Sector-64, Mohali, Punjab-160 062, India

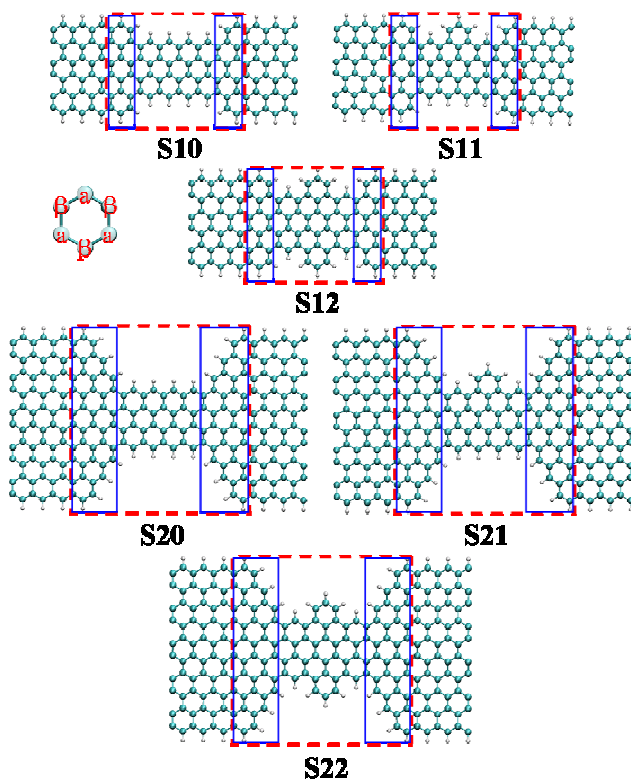


Fig. 1 Schematic diagram of two-probe models about different ZGNR based heterojunction. Group (1) S10, S11 and S12. Group (2) S20, S21 and S22. The parts in the red boxes are the scattering region and the parts outside the red boxes are repeating unit cells for each electrode. Two types of sublattice atoms  $\alpha$  and  $\beta$  are defined in each junction.

GNR junctions.<sup>10</sup> Another important edge modification is protrusion. For example, GNRs may behave like Anderson insulators in the presence of edge disorder and their experimentally measured bandgaps do not depend on orientation.<sup>11</sup> Saloriotta *et al.*<sup>12</sup> showed that the transmission properties of ZGNRs are markedly affected by the protrusion alone while oxygen adsorbate only induce smaller perturbation. An *et al.*<sup>13</sup> investigated that ZGNRs with protrusions show negative differential resistance (NDR) effect. In addition, remarkable edge modifications or edge disorder was found to be induced by substrate. Irregular edges could cause strong backscattering in conductance of AGNRs but ZGNRs have very low sensitivity to edge imperfections and thus are more suitable for connecting electronic components.<sup>14-15</sup>

Besides the insensitivity of conductance of ZGNRs to edge defects, special edge states<sup>17-20</sup> in ZGNRs could bring forth some intriguing phenomena such as zero-conductance resonance<sup>21</sup> and half-metallic conduction.<sup>22</sup> Thus substantial efforts have been made to explore the potential of ZGNRs in constructing basic components in nanocircuit.<sup>14, 15, 23</sup> Especially, much attention has been put on the single channel regime which arises from the contributions of  $\pi$  and  $\pi^*$  bands near the Fermi level ( $E_f$ ).<sup>14, 15, 23</sup> In this regime, ZGNRs show

ballistic transport properties in the presence of substrate-induced disorder<sup>14, 15</sup> and allow high current densities through them with low heat dissipation.<sup>24</sup> To design devices and integrated circuits based on ZGNRs, junctions with different widths should be considered carefully. However, there are still no systematic studies on building blocks of ZGNRs with narrow widths. Narrow ZGNRs show wide single-channel window<sup>14, 15</sup> but are unable to tolerate even a small degree of edge disorder. To design real connecting components in circuits, it is helpful and necessary to understand and predict the transport properties of narrow ZGNRs based heterojunctions with different widths at the atomic level, which is within current experimental scope.<sup>25-27</sup>

## Model and method

We considered transport properties of several wedge-shaped heterojunctions consisting of ZGNRs (up to 2.2 nm in width). They are classified into two groups: junctions with small width difference between the scattering region and the electrode (1) S10, S11, S12; and the ones with large width difference (2) S20, S21, S22, as shown in Fig. 1. Two types of sublattice atoms,  $\alpha$  and  $\beta$ , are defined in this figure for the following discussions. The electrodes of two groups are constituted by ZGNRs with six and ten zigzag chains respectively. The scattering regions of all models are enclosed by red boxes in Fig. 1. All scattering regions were relaxed using density functional theory (DFT) implemented in the SIESTA package<sup>28</sup> before considering their transport properties. Optimization calculations were performed within local density approximation (LDA) and an energy cut off of 150 Ry was used. Valence electrons were expanded in Double- $\zeta$  plus polarization (DZP) and structural relaxations were allowed until the force acting on each atom was less than 0.01 eV/Å. Then transport calculations were performed using DFT combined with the non-equilibrium Green's function (NEGF) formalism as implemented in the TRANSIESTA package.<sup>29</sup> To show the stability of each model, we have presented the the formation energies in the Supporting Information.

## Results and discussion

For ZGNRs in single channel regime,  $\pi$  and  $\pi^*$  bands near  $E_f$  contribute a single conducting channel above and below the  $E_f$ .<sup>14, 15, 23, 30</sup> Thus, the transmission coefficient in this regime equals one. Beyond this regime, subbands away from the  $E_f$  contribute conducting channels. In the following, we mainly focus on the transport properties of ZGNR based heterojunctions within this regime.

To better understand the difference among various heterojunctions, it is instructive to take into account the

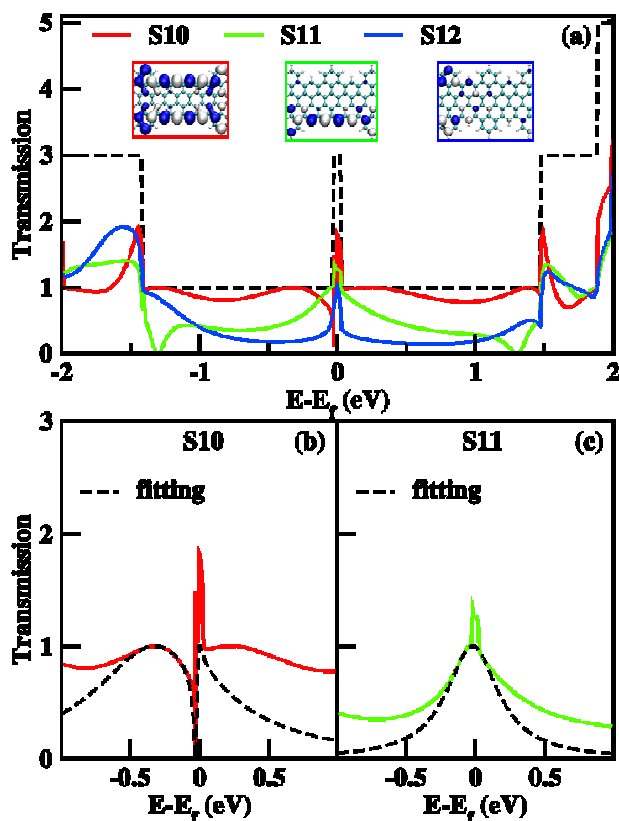


Fig. 2 (a) The black dashed line represents the transmission spectrum of pristine ZGNR based junction while the red, green and blue solid lines are the transmission spectra of S10, S11 and S12. Dominant transmission eigenchannels for three models at  $E_f$  are shown in the inset. (b) and (c) Transmission spectra of S10 and S11 with fitting curves (black dashed line).

transmission spectrum of pristine ZGNR based junction as a reference, indicated by the black dashed line in Fig. 2(a). Since no interface barrier is expected in the pristine case, its transmission function is a step function of the energy representing perfect ballistic transport process. The single channel regime starts from  $-1.41$  eV to  $1.47$  eV.

It is noticed that one peak is present in the narrow region near the  $E_f$  for pristine junction in Fig. 2(a). Such peaks didn't appear in previous tight-binding (TB) calculations which only include the nearest neighbour interaction.<sup>30</sup> In these TB calculations, the partially flat band ( $2\pi/3 \leq |k| \leq \pi$ ) at  $E_f$  barely shows any dispersion.<sup>30</sup> While in transport calculations based on first-principles<sup>13, 31, 32</sup> or tight-binding approach incorporating second nearest neighbour interaction,<sup>15</sup> transmission peaks are observed around  $E_f$  which signifies more than one conducting channel contributing to transmission at this point. In these cases, the flat bands at  $E_f$  are slightly bent and hence, more than one band crossing the  $E_f$  contributes to different conducting channels.

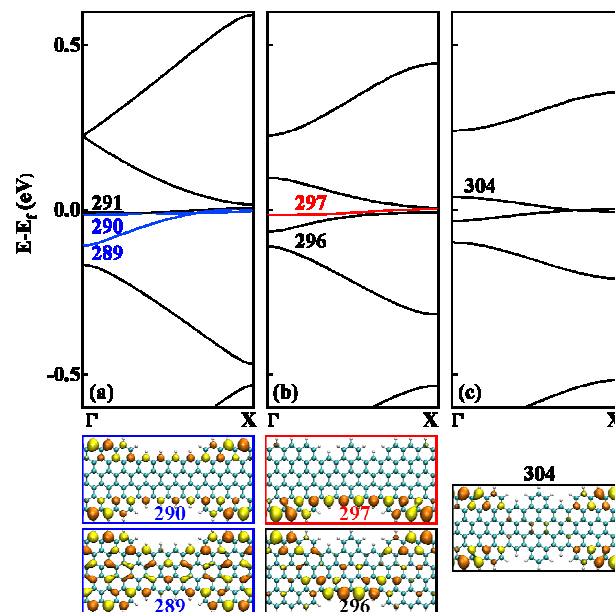


Fig. 3 Electronic band structure for (a) S10; (b) S11; (c) S12 calculated upon assuming periodicity along the transport direction. Selected wave functions are present at bottom. The numbers are band indexes.

#### Junctions with small width difference

The colored lines in Fig. 2 (a) show transmission spectra of non ideal junctions with small interface barriers. We now consider S10 model (red solid line). At a glance, a sharp dip is present just below  $E_f$ . In fact, zero conductance resonance<sup>21, 30</sup> appeared in a similar system in a previous study. Their transmission zeros are related with the imbalance between  $\alpha$  sublattice atoms on the upper side and  $\beta$  sublattice atoms on the lower side of the junction. However, this cannot be accounted for the occurrence of transmission minimum for S10 since perfect balance is shown in the two types of sublattice atoms here. It is noticed that strong asymmetric profile of S10 bears a close resemblance to that of a Fano resonance.<sup>33-39</sup> In Fano resonance model, transmission can be described as<sup>42-44</sup>

$$T(E) = \frac{\Gamma^2}{[E - E_0 - V^2 / (E - E_1)]^2 + \Gamma^2} \quad (1)$$

where  $E_0$  is assumed to be symmetrically coupled to left and right electrodes via the coupling constant  $\Gamma$ ,  $E_1$  is considered to be uncoupled from the electrodes and the coupling between  $E_0$  and  $E_1$  is set to  $V$  (Figure S1(a) in Supporting Information). A comparison between Equation (1) and the ab initio result of S10 is shown in Fig. 2(b). This demonstrates that with an appropriate choice of parameters, Eq. (1) captures the essential features of Fano resonance in S10. The corresponding fitting parameters are  $E_0 = -0.293$  eV,  $E_1 = -0.027$  eV,  $\Gamma = 0.56$  eV, and  $V = 0.089$  eV. The weak coupling strength,  $V$  and a large value  $|E_0 - E_1|/|V| = 2.989$ .

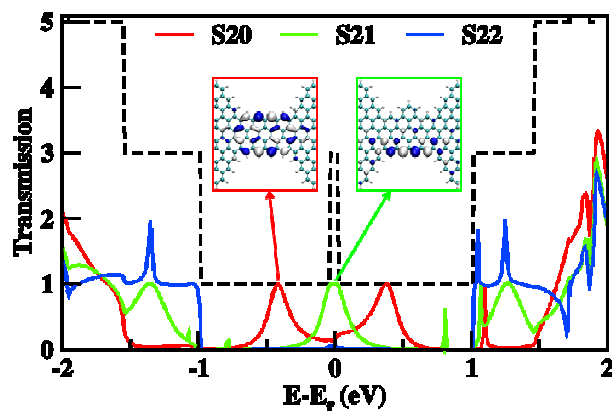


Fig. 4 The black dashed line represents the transmission spectrum of pristine ZGNR based junction while the red, green and blue solid lines are the transmission spectra of models S20 and S21 and S22. Dominant transmission eigenchannels for S20 at  $E = -0.42$  eV and S21 at  $E_f$  are shown in the inset.

These fulfill the condition for Fano resonance given in a recent study.<sup>36</sup> Besides, we have also considered the band structure of S10 in Fig. 3(a). The bands 290 and 289 are coupled to each other near  $E_f$ . The corresponding selected wave functions demonstrate the essential characteristic of these two bands in an intuitive manner. The Fano dip in transmission could be derived from the coupling of a localized edge state (band 290) with an extended state (band 289). The transmission peak at  $E_f$  is supported by edge state (band 290, 291) which is in agreement with dominant transmission eigenchannel analysis<sup>40</sup> at  $E_f$  in Fig. 2(a). In addition, we use double dot model with parallel configuration<sup>50</sup> to fit for the transmission of S10 (see Supporting Information). The fitting parameters fulfil the condition for Fano resonance given in reference 50. Both fitting procedures leads to the same feature and hence it is suitable to use Fano resonance to describe the transmission shape in S10.

Next, we turn our attention to the transport properties of S11 which introduces one protrusion in the central region of model S10. The transmission line (green solid curve in Fig. 2(a)) exhibits a typical Breit-Wigner resonance at  $E_f$ .<sup>42</sup> The fitting of transmission line for S11 is very good as given in Fig. 2(c).<sup>42</sup> The dominant transmission eigenchannel of model S11 at  $E_f$ , which possesses significant weight on pure  $\beta$  sublattice atoms in the lower part of the scattering region. This is also confirmed by band analysis (state of band 297) in Fig. 3(b).

Then, the case of S12 is addressed, which introduces protrusion on both sides of the central region in S10. By inspection of the band (state of band 304) in Fig. 3(c) and the dominant transmission eigenchannel of S12 at  $E_f$  in Fig. 2 (a), a weakly decaying channel is formed at the core of the scattering region and thus it contributes the finite value in the single channel regime. This is different from the research of An *et al.*<sup>13</sup> in which introducing protrusion on both sides results in insulating behaviour and the deviation may be ascribed to the complexity of protrusions in their case.

We also investigated the effect of spin in five different configurations on the transmission spectra of models S10, S11

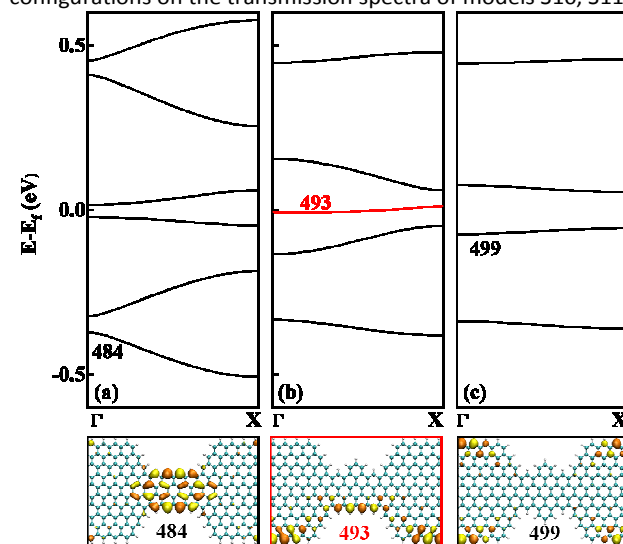


Fig. 5 Electronic band structure for (a) S20; (b) S21; (c) S22 calculated upon assuming periodicity along the transport direction. Selected wave functions are present as insets. The numbers are band indexes.

and S12, as shown in the Supporting Information. Only one spin configuration is found to be efficient in lifting the spin degeneracy in the junctions. The present work outlines the possibility for exploiting the application of spin via destructive quantum interference effect in GNR based devices.

#### Junctions with large width difference

For ZGNR based junctions with large width difference, the single channel regime in Fig. 4 (a) (from  $-0.98$  eV to  $1.01$  eV) is shorter than that in Fig. 2 (a) (from  $-1.41$  eV to  $1.47$  eV), as set by the transmission spectrum of pristine system. This is due to fact that the electrode width of groups (1) is narrower than that of groups (2).<sup>14, 15, 30</sup>

In this regime, a double-peak feature instead of Fano resonance is observed for S20. The two energy states contributing to the transport channels are situated symmetrically away from  $E_f$ . The band analysis in Fig. 5 (a) indicates that the two nearly flat bands near  $E_f$  could support the finite transmission. Yet they are separated from each other. No destructive coupling could be expected between them and no Fano resonance emerges as that in S10.

For S21, a Breit-Wigner resonance persists at  $E_f$ , despite the change in width difference with respect to S11. Discrete peaks appearing in S20 and S21 indicates the effect of more obvious quantum confinement, compared to S11. It should be noticed that fitting gives a better description of the first-principles data in S20 and S21 than that in S11 (see Figure S3 in Supporting Information). This can be understood in the sense that the coupling between the conducting energy level in the scattering region and electrodes is reduced by nearly an order in magnitude from S11 ( $0.226$  eV) to S20 ( $\Gamma_1 = 0.077$  eV, and  $\Gamma_2 = 0.086$  eV) and S21 ( $\Gamma = 0.086$  eV). The weak coupling constants

$\Gamma$  in S20 and S21 satisfy the assumption of independent channel contribution from each conducting energy level for fitting. In addition, the distinct features of transmission for S20 and S21 suggest that edge modification not only affects the numbers of conducting energy level but also the energy alignment between the related level and  $E_f$ ,<sup>41,48,49</sup> which draws a great deal of attention in electrode-molecule-electrode junction. For example, the alignment between a conducting state and  $E_f$  can be controlled by repeated stretching and compressing of single molecule junctions.<sup>48,49</sup> Besides, energy alignment under bias can cause negative differential resistance (NDR).<sup>41</sup>

To gain insight into the essential channels contributing to transmission, the dominant transmitting eigenchannels for S20 at  $E = -0.42$  eV and S21 at  $E_f$  is shown in Fig. 4 (a). Eigen states arising solely from  $\beta$  sublattice atoms contributes the most to the eigenchannel in S21, which is the same as that in S11. However, for S20, extended states from both  $\alpha$  and  $\beta$  sublattice atoms are involved in the eigenchannels. These are in line with band analysis in Fig. 5 (a) and (b), for S20 (state of band 484) and S21 (state of band 493).

Finally, S22 shows good insulating behaviour in the single channel regime. Compared to S12, larger width difference leads to more flat bands in S22 within this regime. Take the band 499 in Fig. 5(c) as an example: wave function of this band indicates no state distributes at the core of the scattering region to support transmission. Both complexity of protrusion and width difference are essential conditions for the presence of insulating behaviour in ZGNR based junction, with comparison to the research of An *et al.*<sup>13</sup>

It is now evident that to tailor the desired transport properties in narrow ZGNRs based heterojunctions, the edge morphology needs to be controlled carefully with atomic precision. S11 (S21) and S22 may serve as the basic component for building logical "1" and "0". The presence of largely asymmetric transmission profile in the vicinity of  $E_f$  in S10 appears to be promising in thermoelectric applications.<sup>46</sup>

## Conclusions

By using *ab initio* methods, we demonstrate a simple but efficient and robust way, involving changes in the width difference between the electrode and the scattering region, and the edge protrusion in the channel, for tailoring distinctive features in transmission function in ZGNRs based junction.

Depending on specific topology of the full carbon  $\pi$  system, the transmission spectra can take on a wide variety of shapes, ranging from Breit-Wigner type line shapes to strongly asymmetric profiles. The interesting charge transport phenomena hold great perspectives regarding the possibility of controlling and manipulating the junction topology.

The richness of the transmission line shape in ZGNRs based junction makes them very attractive for tuning the low energy electrical response and provides a flexible design tool for applications of ZGNRs in real connecting components in nano circuits. The response of the electronic structure of such

junctions<sup>23</sup> to the application of bias is also important, thereby underscoring the need for its exploitation.

## Acknowledgments

This work was supported by a grant from the Research Grants Council of the Hong Kong Special Administrative Region [project No. CityU 103913] and Centre for Functional Photonics of the City University of Hong Kong. The authors thank Dr. Wei Fan for discussion at the early stages of this work.

## Notes and references

- 1 D. M. Sun, M. Y. Timmermans, A. Kaskela, A. G. Nasibulin, S. Kishimoto, T. Mizutani, E. I. Kauppinen and Y. Ohno, *Nature Commun.*, 2013, **4**, 1-8
- 2 L. A. Agapito and N. Kioussis, *J. Phys. Chem. C*, 2011, **115**, 2874-2879.
- 3 A. H. C. Neto, F. Guinea, N. M. R. Peres, K. S. Novoselov, and A. K. Geim, *Rev. Mod. Phys.*, 2009, **81**, 109-162.
- 4 Y. W. Son, M. L. Cohen and S. G. Louie, *Phys. Rev. Lett.*, 2006, **97**, 216803.
- 5 Z. F. Wang, Q. X. Li, H. X. Zheng, H. Ren, H. B. Su, Q. W. Shi, and J. Chen, *Phys. Rev. B*, 2007, **75**, 113406.
- 6 O. Hod, V. Barone, J. E. Peralta and G. E. Scuseria, *Nano Lett.*, 2007, **7**, 2295-2299.
- 7 G. Lee, and K. Cho, *Phys. Rev. B*, 2009, **79**, 165440.
- 8 H. X. Zheng, and W. Duley, *Phys. Rev. B*, 2008, **78**, 045421.
- 9 B. Biel, F. Triozon, X. Blase, and S. Roche, *Nano Lett.*, 2009, **9**, 2725-2729.
- 10 S. M. M. Dubois, A. Lopez-Bezanilla, A. Cresti, F. Triozon, B. Biel, J. C. Charlier and S. Roche, *ACS Nano* 2010, **4**, 1971-1976.
- 11 D. Querlioz, Y. Apertet, A. Valentin, K. Huet, A. Bournel, S. Galdin-Retailleau and P. Dollfus, *Appl. Phys. Lett.*, 2008, **92**, 042108.
- 12 K. Saloritta, Y. Hancock, A. Kärkkäinen, L. Kärkkäinen, M. J. Puska and A. P. Jauho, *Phys. Rev. B*, 2011, **83**, 205125.
- 13 Y. P. An, W. Ji and Z. Q. Yang, *J. Phys. Chem. C*, 2012, **116**, 5915-5919.
- 14 D. A. Areshkin, D. Gunlycke and C. T. White, *Nano Lett.*, 2007, **7**, 204-210.
- 15 D. A. Areshkin, and C. T. White, *Nano Lett.*, 2007, **7**, 3253-3259.
- 16 W. Long, Q. F. Sun and J. Wang, *Phys. Rev. Lett.*, 2008, **101**, 166806.
- 17 M. Fujita, K. Wakabayashi, K. Nakada, and K. Kusakabe, *J. Phys. Soc. Jpn.*, 1996, **65**, 1920-1923.
- 18 K. Nakada, M. Fujita, G. Dresselhaus and M. S. Dresselhaus, *Phys. Rev. B*, 1996, **54**, 17954-17961.
- 19 K. Wakabayashi, M. Fujita, H. Ajiki and M. Sigrist, *Phys. Rev. B*, 1999, **59**, 8271-8282.
- 20 Y. Miyamoto, K. Nakada and M. Fujita, *Phys. Rev. B*, 1999, **59**, 9858-9861.
- 21 K. Wakabayashi and M. Sigrist, *Phys. Rev. Lett.*, 2000, **84**, 3390-3393.
- 22 Y. W. Son, M. L. Cohen and S. G. Louie, *Nature*, 2006, **444**, 347-349.
- 23 Z. Y. Li, H. Y. Qian, J. Wu, B. L. Gu and W. H. Duan, *Phys. Rev. Lett.*, 2008, **100**, 206802.
- 24 D. Gunlycke, H. M. Lawler and C. T. White, *Phys. Rev. B*, 2007, **75**, 085418.
- 25 J. M. Cai, *et al. Nature*, 2010, **466**, 470-473.
- 26 P. Merino, *et al. Nat. Commun.*, 2014, **5**, 3054.

## ARTICLE

## Nanoscale

- 27 Y.-C. Chen, *et al. Nat. Nanotechnol.*, 2015, **10**, 156-160
- 28 J. M. Soler, E. Artacho, J. D. Gale, A. García, J. Junquera, P. Ordejón, and D. S.-Portal, *J. Phys.: Condens. Matter*, 2002, **14**, 2745-2779.
- 29 M. Brandbyge, J. L. Mozos, P. Ordejón, J. Taylor and K. Stokbro, *Phys. Rev. B*, 2002, **65**, 165401.
- 30 K. Wakabayashi, *Phys. Rev. B*, 2001, **64**, 125428.
- 31 B. Biel, X. Blase, F. Triozon, and S. Roche, *Phys. Rev. Lett.*, 2009, **102**, 096803.
- 32 Z. F. Hou and M. Yee, *IEEE-NANO 7th IEEE Conference*, 2007, 554-557.
- 33 U. Fano, *Phys. Rev.*, 1961, **124**, 1866-1878.
- 34 X. F. Qian, J. Li and S. Yip, *Phys. Rev. B*, 2010, **82**, 195442.
- 35 T. A. Papadopoulos, I. M. Grace and C. J. Lambert, *Phys. Rev. B*, 2006, **74**, 193306.
- 36 D. Nozaki, H. Sevinçli, S. M. Avdoshenko, R. Gutierrez, and G. Cuniberti, *Phys. Chem. Chem. Phys.*, 2013, **15**, 13951-13958.
- 37 X. Q. Shi, Z. X. Dai and Z. Zeng, *Phys. Rev. B*, 2007, **76**, 235412.
- 38 S. K. Min, W. Y. Kim, Y. Cho and K. S. Kim, *Nat. Nanotechnol.*, 2011, **6**, 162-165.
- 39 Y. Cho, S. K. Min, W. Y. Kim and K. S. Kim, *Phys. Chem. Chem. Phys.*, 2011, **13**, 14293-14296.
- 40 M. Paulsson and M. Brandbyge, *Phys. Rev. B*, 2007, **76**, 115117.
- 41 W. Fan, R. Q. Zhang, A. Reily Rocha, and S. Sanvito, *J. Chem. Phys.*, 2008, **129**, 074710.
- 42 C. J. Lambert, *Chem. Soc. Rev.*, 2015, **44**, 875-888.
- 43 J. C. Cuevas and E. Scheer, *Molecular Electronics: An Introduction to Theory and Experiment* World Scientific, Singapore, 1st ed, 2010.
- 44 Y. Kim, A. Garcia-Lekue, D. Sysoiev, T. Frederiksen, U. Groth and E. Scheer, *Phys. Rev. Lett.*, 2012, **109**, 226801.
- 45 R. Stadler and T. Markussen, *J. Chem. Phys.*, 2011, **135**, 154109.
- 46 T. Markussen, R. Stadler and K. S. Thygesen, *Phys. Chem. Chem. Phys.*, 2011, **13**, 14311-14317.
- 47 G. D. Mahan and J. O. Sofo, *Proc. Natl. Acad. Sci. USA*, 1996, **93**, 7436-7439.
- 48 Y. H. Tang, V. M. K. Bagci, J. H. Chen and C. C. Kaun, *J. Phys. Chem. C*, 2011, **115**, 25105-25108.
- 49 C. Bruot, J. Hihath and N. J. Tao, *Nat. Nanotechnol.*, 2012, **7**, 35-40.
- 50 M. L. L. de Guevara, F. Claro and P. A. Orellana, *Phys. Rev. B*, 2003, **67**, 195335.